LANGMUIR

pubs.acs.org/Langmuir Article

Excellent Protein Immobilization and Stability on Heterogeneous C−TiO_2 Hybrid Nanostructures: A Single Protein AFM Study

Yihui Dong, Xiaoyan Ji,* Aatto Laaksonen, Wei Cao, Hongyan He, and Xiaohua Lu*

Cite This: *Langmuir* 2020, 36, 9323−9332 Read Online

ACCESS | Metrics & More | Article Recommendations | Supporting Information

ABSTRACT: Enhancing molecular interaction is critical for improving the immobilization and stability of proteins on TiO_2 surfaces. In this work, mesoporous TiO_2 materials with varied pore geometries were decorated with phenyl phosphoric acid (PPA), followed by a thermal treatment to obtain chemically heterogeneous C−TiO_2 samples without changing the geometry and crystalline structure, which can keep the advantages of both carbon and TiO_2. The molecular interaction force between the protein and the surfaces was measured using atomic force microscopy by decomposing from the total adhesion forces, showing that the surface chemistry determines the interaction strength and depends on the amount of partial carbon coverage on the TiO_2 surface (~40−80%). Samples with 58.3% carbon coverage provide the strongest molecular interaction force, consistent with the observation from the detected friction force. Surface-enhanced Raman scattering and electrochemical biosensor measurements for these C−TiO_2 materials were further conducted to illustrate their practical implications, implying their promising applications such as in protein detection and biosensing.

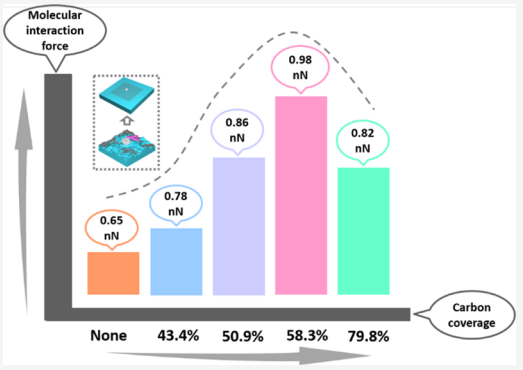

1. INTRODUCTION

The development of nano-biomaterials with high conductivity, high stability, and good biocompatibility has become an active research topic in the past decades.[1,2] Among many materials, titanium oxide (TiO_2) is particularly promising because of its structural stability and excellent biocompatibility.[3,4] It has been used in a large variety of applications and is found suitable in manufacturing nano-biomaterials. However, TiO_2 materials have problems of low detection sensitivity and a weak signal for protein detection because TiO_2 is a semiconductor material with low conductivity. Besides, the stability of the immobilized biomolecules on surfaces is also important in evaluating the performance of biomaterials.[5,6] How to achieve a high loading coupled with good stability of biomolecules is another important research topic.[7] However, when using TiO_2 materials, the hydroxyl groups (−OH) on their surface make it easy to form a strongly bounded hydration layer, leading to difficulties to immobilize biomolecules *via* weak van der Waals interactions.[8,9]

To improve the performance of TiO_2, surface modifications have been used to increase the conductivity and enhance the immobilization and stability of biomolecules on the surface. It has been found that surface chemical modifications, such as covalent bonding, cross-linking, and grafting, can be used to increase the immobilization and stability of the biomolecules.[10,11] However, some unexpected side effects such as weakening of the biomolecule response[12] or irreversible deactivation may occur.[13] Previous research has shown that the pore structure of the TiO_2 surface is highly important for the immobilization and stability of biomolecules.[6,14,15] Therefore, surface modification may weaken its positive effect. Hence, a surface modification that enhances stability while maintaining the geometric properties of TiO_2 is highly desirable.

Of different materials that can be used to modify the surface of TiO_2, carbon is particularly important, improving the electrochemical activity and conductivity.[16,17] For example, surface modification to form hybrid TiO_2−carbon materials has been used to improve the conductivity of TiO_2.[18−20] These hybrid materials may show simultaneously both the electron conductivity of carbon and the corrosion resistance of metal oxides. However, in most of the previous works, the carbon-modified TiO_2 was fully covered by carbon, potentially reducing the advantages of TiO_2, and the immobilization and stability of the biomolecules on the surface were decreased.[21,22] Therefore, a partial or heterogeneous coverage by carbon of the TiO_2 surface can be an effective way to maintain the combined advantages of both carbon and TiO_2. Much research has been conducted to study hybrid TiO_2−carbon and its biological performance[23−25] but with the focus on the electric

Received: July 1, 2020
Published: July 16, 2020

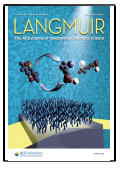

https://dx.doi.org/10.1021/acs.langmuir.0c01942
Langmuir 2020, 36, 9323−9332

conductivity. It is still unclear, however, how the nature of the carbon coverage will quantitatively affect the immobilization and stability of biomolecules and what is the intrinsic mechanism behind the stability enhancement offered by TiO_2 when covered with carbon. For example, some studies indicate that the structural parameters of the materials have a significant impact on the immobilization and stability of the biomolecules,[6,14,26] while others indicate that the surface charges and surface modification have a dominating impact.[27] Therefore, understanding which factors and how they affect the immobilization and stability of the biomolecules is needed.

To evaluate the immobilization and stability is of great importance. Principally, both the immobilization and stability of biomolecules on the surface are determined by inter- and intramolecular interactions. It is not adequate to evaluate the interactions of biomolecules with the solid-surface based on the adsorption capacity, electrical signals, and so forth in the macroscale to determine the interaction strength. Determination of the interactions at the microscale is needed. In our previous work, we did propose an atomic force microscopy (AFM)-based method to quantify the force between a single protein molecule and the TiO_2 surfaces.[28−30] However, how to apply this method to study the effect of surface chemical properties of TiO_2 and from that identify the key impactors affecting the immobilization and stability of the biomolecules is still not yet clear.

In this study, our main purpose is to investigate the effect of the geometrical topography and surface chemistry of TiO_2 on the immobilization and stability of biomolecules by quantifying the interaction strength of biomolecules on the TiO_2 surface. In the current study, mesoporous TiO_2 materials featuring different pore structures and modified with carbon by PPA did serve as the model support and lysozyme was chosen as the model of the adsorbed protein. We study how the coverage of carbon on the TiO_2 surface changes the molecular interaction forces in the AFM-measured adhesion force and which factors (*e.g.*, geometry, modification) are dominant in affecting the molecular interaction force to provide us knowledge of enhancing the immobilization and stability of biomolecules on the surface. The friction force was further conducted to verify the effect of carbon on the molecular interaction force. Meanwhile, the surface-enhanced Raman scattering (SERS) and electrochemical biosensor measurements were further used to illustrate the practical implications of these C−TiO_2 materials for protein detection and biosensing.

2. EXPERIMENTAL SECTION

2.1. Materials. Lysozyme was purchased from BioDee BioTech Co. Ltd. (Beijing, China). Phenyl phosphoric acid (PPA, $C_6H_7O_2P$) and 16-mercaptohexadecanoic acid ($HS(CH_2)_{15}COOH$) were purchased from Sigma-Aldrich Trading Co. Ltd. (Shanghai, China). *N*,*N*-Dimethyl formamide (*N*,*N*-DMF, anhydrous), triethylamine ($C_6H_{15}N$), and trifluoroacetic anhydride ($C_4F_6O_3$) were purchased from J&K Scientific Ltd. (Shanghai, China). Dichloromethane (CH_2Cl_2) was purchased from Sinopharm Chemical Reagent Co. Ltd., (Shanghai, China). Deionized water was used in all the experiments.

2.2. Carbon Modification of Mesoporous TiO_2. The mesoporous TiO_2 materials were fabricated from the potassium dititanate ($K_2Ti_2O_5$) fibers as described in our previous work.[31,32] The ion exchanging products ($H_2Ti_2O_5$) were sintered at 300, 500, 600, and 700 °C, respectively, with a heating rate of 2 °C·min^{-1} for 2 h and then naturally cooled to the room temperature in the furnace. These prepared mesoporous TiO_2 samples were named as T300, T500, T600, and T700, respectively.

Different agents can be used for carbon modification, among which the silane coupling agent is the most conventional modifier. However, it has been pointed out that the silicone-based coupling agent molecules are very sensitive to water on the TiO_2 surface and are highly prone to self-agglomeration, weakening the modification effect.[33] The organic phosphine-based coupling molecules (such as phenyl phosphoric acid, PPA) show high resistance to the water effect. Considering the mesoporous TiO_2 materials with strong hydrophilicity, it is more suitable to use an organic phosphine coupling agent to adjust its surface properties, and in this work, PPA was chosen as the modifier. The modification processes were divided into two steps: (a) grafting of PPA onto TiO_2 to obtain a PPA surface-modified sample PPA−TiO_2; (b) thermal treatment of PPA−TiO_2 to obtain a carbon surface-modified sample C−TiO_2. Specifically, 1.131 g of PPA and 3 g of mesoporous TiO_2 were dissolved in the 60 mL of dichloromethane at room temperature with violent stirring. After stirring for 24 h, the sediments were obtained with filtration and washed with the acetone-deionized water (volumetric ratio of 1:1) three times to remove the residual PPA/dichloromethane, and then the products were dried in a desiccator at 100 °C. Finally, PPA−T300, PPA−T500, PPA−T600, and PPA−T700 were sintered at 500 °C with a heating rate of 2 °C·min^{-1} and kept for 6 h under the N_2 atmosphere. The final modification products were designated as C−T300, C−T500, C−T600, and C−T700.

2.3. Characterization. The mesoporous TiO_2 and C−TiO_2 samples were transferred into a clean vial for N_2 adsorption−desorption measurements (Micromeritics TriStar II 3020). The crystalline phases were determined with a Raman spectrometer (HORIBA LabRAM HR 800) equipped with a He-Cd laser. The weight loss of the samples was detected with the thermogravimetric analysis (TGA, Model SDT 2960).

2.4. Lysozyme Adsorption Assays. Approximately 20 mL of lysozyme solution (1 mg·mL^{-1}) was obtained by dissolving the protein in the 0.05 M, pH = 10.0 buffer solution. A series of mesoporous TiO_2 (T300, T500, T600, T700) and C−TiO_2 (C−T300, C−T500, C−T600, C−T700) samples (200 mg) were suspended in the protein solution in closed centrifuge tubes. The mixtures in the centrifuge tubes were shaken at 30 °C at 180 rpm for 72 h to ensure reaching the equilibrium. To obtain the amounts of lysozyme molecules adsorbed on the mesoporous TiO_2 and C−TiO_2 at equilibrium, the adsorption mixture was transferred to the microcentrifuge tubes and spun at 8000 rpm for 10 min, and the supernatant concentration of lysozyme was determined by measuring the lysozyme absorbance with a UV−vis spectrophotometer at λ = 280 nm. The amount of lysozyme bound to TiO_2 was calculated from the difference in the initial and final protein concentrations.

2.5. Protein Immobilization on Self-Assembled Monolayer-Functionalized AFM Tip. The AFM (model: NPG-10, Si_3N_4, tip radius as 20 nm) tips, coated with gold, were immersed in 50 mL of 1 mM $HS(CH_2)_{15}COOH$ solution (the volumetric fraction of a 50% ethanol solution) and maintained under dark conditions in an incubator at 37 °C for 12 h. Then, the tips were washed with ethanol three times and dried with nitrogen. After that, the tips were immersed in a mixture of *N*,*N*-DMF (9.58 mL), triethylamine (0.28 mL), and trifluoroacetic anhydride (0.14 mL) for approximately 20 min.[34] After that, the tips were washed with dichloromethane three times and dried with nitrogen. At last, the tips were immersed in the 5 mg·mL^{-1} lysozyme buffer solution for 12 h, washed with the buffer solution, and dried with nitrogen.

2.6. AFM Measurements. The adhesion force measurements were performed with AFM (Bruker, Dimension ICON) in contact mode at room temperature. The lysozyme-modified tips with normal spring constants between 0.06 and 0.35 N·m^{-1} were used throughout the experiments, and the scan rate was 1.00 Hz. The normal spring constant of the tip was calibrated using the deflection sensitivity of the supported cantilever to transform the normal load signals from volts (V) into the true normal load (N). The calibration of tips was

https://dx.doi.org/10.1021/acs.langmuir.0c01942
Langmuir 2020, 36, 9323−9332

performed with the thermal tune method in air over a sapphire substrate at room temperature. The adhesion forces were measured with the force−distance curve approach, and 50 force−distance curves at the maximal adhesion force upon retraction were recorded at multiple randomly chosen spots for analysis.

The friction force measurement was performed under the same applied load of 1 V, using lateral force images, derived from trace and retrace tracks of 2 × 2 μm^2 under the tip at a 90° scan angle to the cantilevers long the axis (scan rate: 1 Hz). The average lateral force was given in terms of an output voltage signal, which is half-difference of the average lateral deflection signal on the photodetector of the forward and reverse traces. The friction results presented here are the average of five measurements at independent multiple sample positions.

2.7. SERS Measurements. TiO_2 and C−TiO_2 samples chosen as the substrates for Raman spectroscopic studies were separately soaked in the 5 × 10^{-4} M Cyt C solution [0.1 M phosphate buffer saline solution, pH = 7.2] at 4 °C for 2 h. The SERS spectrum was obtained using a HORIBA-Jobin Yvon system (HORIBA LabRAM HR800) with a 514 nm air-cooled Ar^+ laser line. The laser power was controlled at ∼5 mW. The typical spectral collection condition was set to be 20 s of exposure time and two accumulations.

3. RESULTS AND DISCUSSION

3.1. Mesoporous TiO_2 and C−TiO_2 Characterization. The carbon heterogeneous modification process included the grafting of PPA onto TiO_2 to obtain PPA−TiO_2 and the thermal treatment to obtain C−TiO_2 as illustrated in Figure 1.

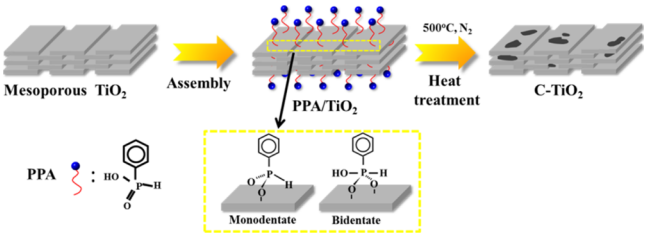

Figure 1. Schematic representation of the surface modification of mesoporous TiO_2 employing PPA as a modifier.

The selected modifier PPA was grafted onto the sample surface by bonding its phosphoric-based group with the hydroxyl group on the TiO_2 surfaces,[35] and the hydroxyl group of TiO_2 was replaced with the carbon after the thermal treatment.

Figure 2a shows Raman spectra (ranging from 100 to 1200 cm^{-1}) of the mesoporous TiO_2 and the corresponding C−TiO_2 samples. All of the samples exhibit the characteristic bands at the frequencies of 144.6, 397.7, 515.7, and 640.8 cm^{-1} (marked with a solid square in Figure 2a), which represent the pure anatase TiO_2 nanocrystals both for mesoporous-TiO_2 and C−TiO_2 samples. Figure 2b shows the local-Raman spectra (ranging from 1200 to 2000 cm^{-1}) in order to identify the existence and type of carbon on the C−TiO_2 samples. The G-band at approximately 1600 cm^{-1} is usually assigned to the E_{2g} phonon of C sp^2 atoms, and the D-band at approximately 1340 cm^{-1} is a breathing mode of *k*-point phonons of A_{1g} symmetry,[36] which implies that the D-band and G-band represent the peaks of amorphous and graphene types of carbon, respectively. These observations demonstrated the coexistence of amorphous carbon and graphene on the surface of C−TiO_2. No such peak can be observed for the mesoporous TiO_2. Meanwhile, the results from the Fourier transform infrared (FT-IR) spectra demonstrated the PPA could be self-assembled into the TiO_2 surface and the organic composition of benzene can be transformed into carbon (Figure S1a). Three peaks (O 1s, Ti 2p, and C 1s) were observed in the X-ray photoelectron spectroscopy (XPS) pattern of C−TiO_2 (Figure S1b), and the percentages of Ti, O, and C elements were 22.4, 56.4, and 21.2%, respectively, which indicated that the modification species did not completely cover the TiO_2 surface. The values of the isoelectric point (IEP) for the mesoporous TiO_2 and C−TiO_2 samples were obtained from the zeta potential pH titration curves (Figure S2), and the results are about 4.5 for mesoporous TiO_2 but 3.5 for C−TiO_2 as listed in Table 1. The reduction of IEPs is due to the existence of the surface carbon incorporation after modification, which may alter electrophoretic mobility.

Table 1. Structural Parameters and IEPs of Mesoporous TiO_2 and C−TiO_2 Measured by BET and Zeta Potential Measurements

sample	[a] β, nm	[b] S_T, $m^2 \cdot g^{-1}$	[c] V_m, $cm^3 \cdot g^{-1}$	[d] IEP
T300/C−T300	8.6/8.0	216.4/213.4	0.40/0.40	4.4/3.3
T500/C−T500	15.5/15.1	96.7/96.1	0.37/0.36	4.7/3.4
T600/C−T600	24.4/24.0	59.3/59.3	0.37/0.36	4.5/3.5
T700/C−T700	31.9/32.4	28.8/28.5	0.20/0.20	4.5/3.5

[a] β: pore size, nm. [b] S_T, BET surface areas, $m^2 \cdot g^{-1}$. [c] V_m: pore volume, $cm^3 \cdot g^{-1}$. [d] IEP: isoelectric point.

It is well known that the hydrophilicity of TiO_2 is due to the high concentration of hydroxyl groups on the surfaces, and the densities of the hydroxyl groups on the mesoporous TiO_2 and C−TiO_2 surfaces can be determined based on TGA measurements. In this work, TGA under the N_2 flow was conducted for

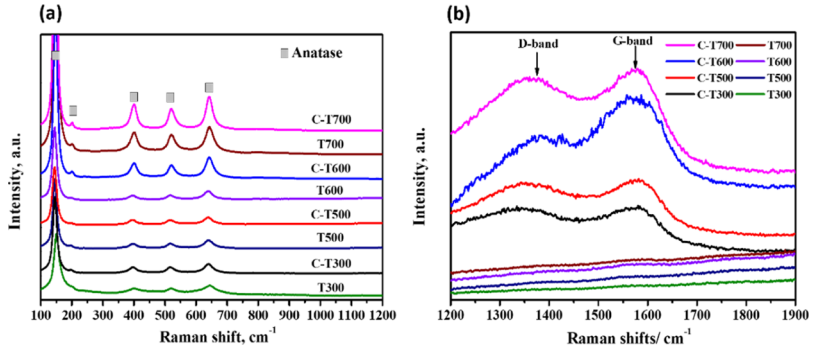

Figure 2. (a) Raman spectrum of mesoporous TiO_2 and C−TiO_2 specimens ranging from 100 to 1200 cm^{-1}. (b) Local-Raman spectrum of C−TiO_2 and mesoporous TiO_2 specimens ranging from 1200 to 2000 cm^{-1}.

https://dx.doi.org/10.1021/acs.langmuir.0c01942
Langmuir 2020, 36, 9323−9332

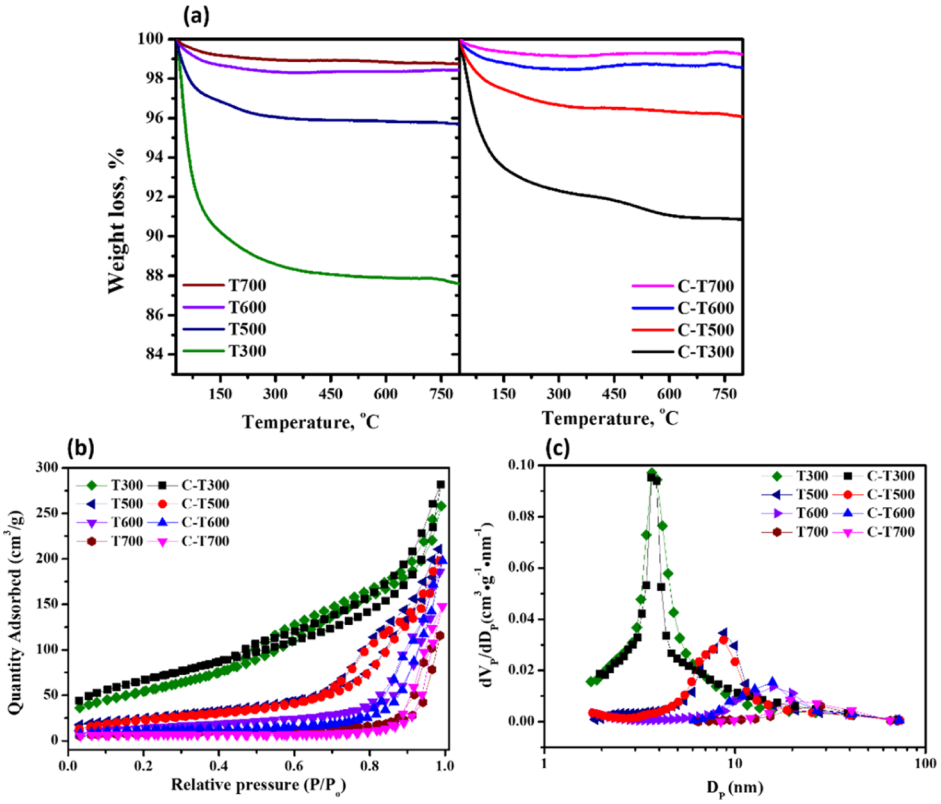

Figure 3. (a) TGA experiments of mesoporous TiO_2 and C−TiO_2 samples sintered at different temperatures. (b) N_2 adsorption−desorption isotherms and (c) pore size distribution curves of sintered mesoporous TiO_2 and corresponding C−TiO_2 samples.

both mesoporous TiO_2 and C−TiO_2 with different pore structures. The results are shown in Figure 3a. Here, the total weight losses were attributed to the weight of water molecules adsorbed on TiO_2 surfaces and the hydroxyl group on TiO_2 surfaces, which can also be regarded as the determination of the densities of the hydroxyl group on TiO_2 surfaces. As shown in Figure 3, the values of distinct reduction in the total weight loss for T300, T500, T600, and T700 were approximately 12.1, 4.2, 1.7, and 1.2%, respectively. It indicates different densities of the hydroxyl groups for different TiO_2 samples, and T300 prepared at low temperature has the highest value among the four mesoporous TiO_2 samples. Therefore, the density of the hydroxyl groups decreases with the increase of calcination temperature. Meanwhile, the values of distinct reduction in the total weight loss for C−T300, C−T500, C−T600, and C−T700 were approximately 9.1, 3.8, 1.4, and 0.8%, respectively. Therefore, the density of the hydroxyl groups on the C−TiO_2 was decreased after the carbon modification compared with that for mesoporous TiO_2. As the reduction of the hydroxyl groups will mitigate the water adsorption, the carbon modification can also be considered as one kind of hydrophobic treatment.

TiO_2 is hydrophilic and carbon is hydrophobic. In order to further verify whether the surface modification is heterogeneous instead of full-coverage, the hydrophilic H_2O and hydrophobic CCl_4 were chosen as the mixed solvents to investigate and compare the dispersibilities of the mesoporous-TiO_2 and C−TiO_2. The investigation shows that the mesoporous-TiO_2 sample was only suspended in H_2O, whereas the C−TiO_2 sample was suspended in both H_2O and CCl_4 (Figure S3). It indicates again that this carbon modification forms a heterogeneous surface, exposing both the hydrophobic and hydrophilic parts. The content of PPA obtained by X-ray fluorescence (XRF) listed in Table S1 showed that the content of P_2O_5 in PPA−TiO_2 was basically the same as that in C−TiO_2 after heat treatment, indicating that there is no volatile loss of phosphorus during the heat treatment. Hence, the carbon coverages on C−TiO_2 were estimated through the amount of phosphorus and calculated from the XRF data (Table S1) after the grafting of PPA at room temperature. The results showed that the TiO_2 surface is occupied by the carbon species with a value of 43.4%, which further verified that this modification is heterogeneous.

The N_2 adsorption−desorption isotherm is displayed in Figure 3b, for both the mesoporous TiO_2 and the corresponding C−TiO_2 samples, showing a typical isotherm of type-IV and indicating the presence of well-developed mesopores in those samples. The average pore size (β in nm), BET surface area (S_T in $m^2 \cdot g^{-1}$), and the pore volume (V_m in $cm^3 \cdot g^{-1}$) are summarized in Table 1. The average pore sizes for T300, T500, T600, and T700 are around 8.6, 15.5, 24.4, and 31.9 nm, respectively, and increase with increasing the calcined temperature in preparation. On the contrary, the BET surface area decreases significantly from 216.4 $m^2 \cdot g^{-1}$ for T300 to 59.3 $m^2 \cdot g^{-1}$ for T700, and the pore volume also decreases but not remarkably. This indicates that the decrease of the surface area is not from the pore collapse.

Compared to the mesoporous TiO_2, the structure parameters of the C−TiO_2 samples are unchanged, as listed in Table 1. The overlap of the pore-size distributions in Figure 3c further indicates the same pore structures of mesoporous-TiO_2 and C−TiO_2. Meanwhile, the scanning electron microscopy (SEM) and transmission electron microscopy (TEM) results (see Figure S4, T500 as an example) also

https://dx.doi.org/10.1021/acs.langmuir.0c01942
Langmuir 2020, 36, 9323−9332

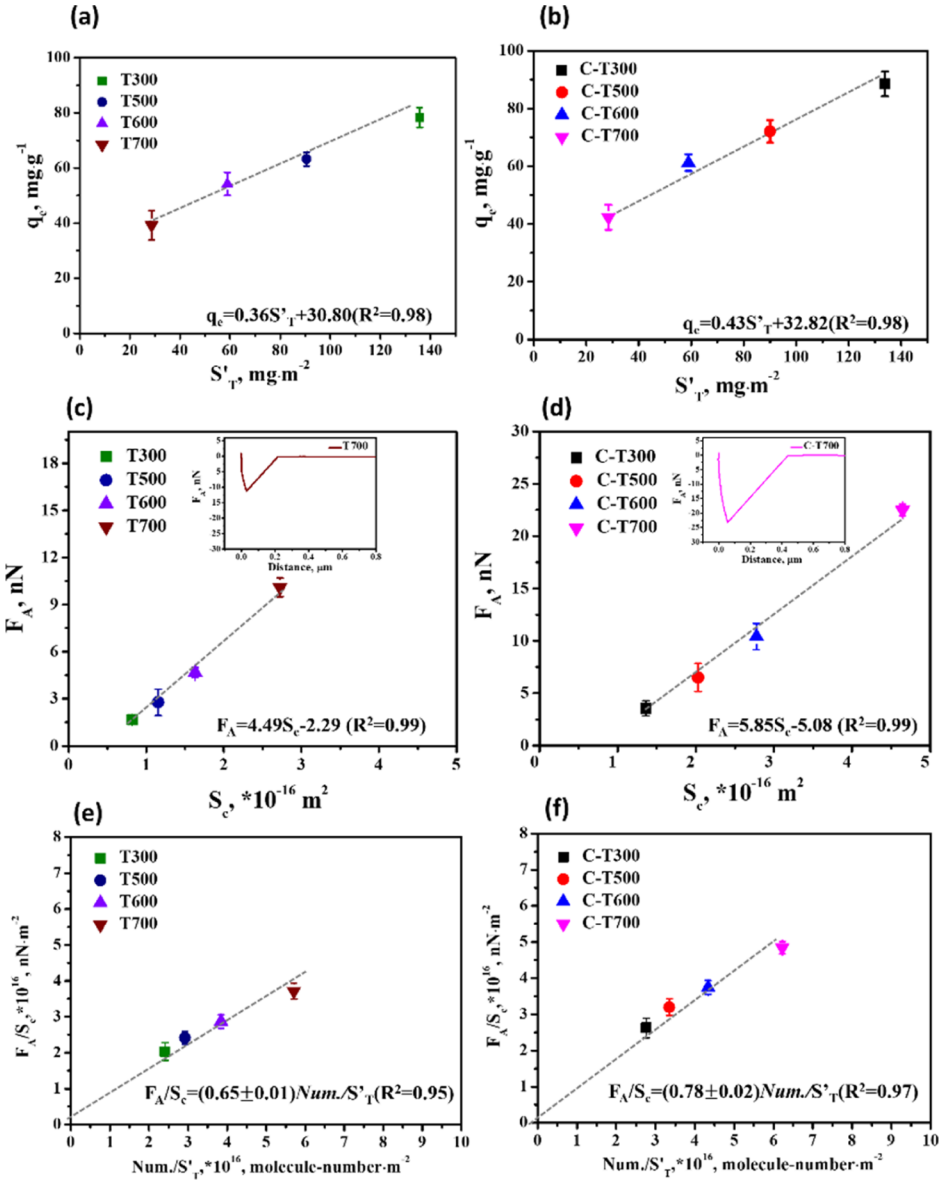

Figure 4. Linear relationships between the adsorption amount of lysozyme on (a) mesoporous TiO_2, (b) C−TiO_2 samples and the effective surface area, respectively; the linear relationships between the adhesion force of lysozyme on (c) mesoporous TiO_2, (d) C−TiO_2 samples and the contact area, respectively; insets: typical force−distance curves for lysozyme on (c) TiO_2 (T700 as an example) and (d) C−TiO_2 (C−T700 as an example); adhesion force of lysozyme interacting with (e) mesoporous TiO_2; (f) C−TiO_2 per unit area *vs* the number of adsorbed lysozyme molecules per unit area.

indicated that both the PPA modification and thermal treatment for carbon forming would not change the pore structure of TiO_2. Therefore, combined with the results above, we can conclude that the modification only changes the surface chemistry without influencing the geometric and crystal structures of the materials.

3.2. Quantification of the Adsorption Capacity. To study the protein interaction with heterogeneous carbon modification in C−TiO_2 where both the adsorption capacity and adhesion force needed to be measured, lysozyme was chosen as a model protein because it is a rigid globular protein and stabilized during the adsorption without changing the conformation at various conditions. The equilibrium adsorption amounts of lysozyme (q_e in mg·g^{-1}) on T300, T500, T600, and T700 were measured with the values of 78.3, 63.2, 54.2, and 39.2 mg·g^{-1}, respectively, and those on C−T300, C−T500, C−T600, and C−T700 are 88.5, 72.1, 61.2, and 42.3 mg·g^{-1}, respectively. Comparing the adsorption capacities of lysozyme adsorbed on either TiO_2 or C−TiO_2 with different geometrical structures, it shows that various pore structures provide different surface areas and thus vary the adsorption of lysozyme. For example, T300 (or C−T300) possesses the largest surface area and then achieves the highest adsorption capacity, whereas T700 (or C−T700) with the smallest surface area achieves the lowest adsorption capacity. The different adsorption capacities for TiO_2 and C−TiO_2 with the same pore structures may be related to the surface chemical properties. For further comparison and analysis, the adsorption amounts of lysozyme on TiO_2 and C−TiO_2 per unit surface area were estimated.

In order to obtain the adsorption amounts of lysozyme per unit surface area, the BET surface areas (S_T in m^2·g^{-1}) of these

https://dx.doi.org/10.1021/acs.langmuir.0c01942
Langmuir 2020, 36, 9323−9332

mesoporous TiO_2 and C−TiO_2 were deducted by the surface areas provided by the size smaller than the size of lysozyme to obtain the effective surface area (S'_T in $m^2 \cdot g^{-1}$). In this work, the effective size of the lysozyme was equal to its geometric size because the pH condition was under the pI of lysozyme, that is, lysozyme was neutral. Then, we established the relationship between S'_T and q_e, as shown in Figure 4a,b. The linear relationships show that the adsorption amount per unit area is proportional to the effective surface area provided by the samples. The values of q_e/S'_T were converted to Num./S'_T by dividing by the molecular weight of lysozyme and multiplying by Avogadro's number. The values of Num./S'_T are 2.41×10^{16}, 2.92×10^{16}, 3.84×10^{16}, and 5.71×10^{16} molecule-number$\cdot m^{-2}$ for T300, T500, T600, and T700, respectively. For C−T300, C−T500, C−T600, and C−T700, the values of Num./S'_T are 2.76×10^{16}, 3.35×10^{16}, 4.34×10^{16}, and 6.22×10^{16} molecule-number$\cdot m^{-2}$, respectively.

It was found that the adsorption amount per unit area of lysozyme on C−TiO_2 is larger than that on the mesoporous TiO_2. Based on the foregoing section, the effective surface area of C−TiO_2 was almost the same before the surface modification, that is, the modification did not change the surface pore structure, and thus the change of the adsorption amount per unit area should result from the change of the surface chemical properties. This observation can be explained based on following three reasons: (1) the TiO_2 surface with the hydroxyl groups presented on the TiO_2 surface adsorbs enzymes only with weak van der Waals interactions,[9,37] while the hydroxyl groups increase the hydration of TiO_2, hindering lysozyme moving close to the surface.[38] Therefore, the higher the density of hydroxyl groups, the lower the adsorption capacity. As the modification with carbon decreases the density of hydroxyl groups presented on the TiO_2 surface, the adsorption amount per unit area on C−TiO_2 is higher. (2) The zeta potential measurements showed that the IEP of mesoporous TiO_2 decreased after the carbon modification, indicating that C−TiO_2 carries negative charges, resulting in relatively strong electrostatic interactions with lysozyme. Thus, the adsorption increases. (3) As discussed in the foregoing section, the carbon modification is also a partially hydrophobic treatment, and the hydrophobic surface is more attractive for protein adsorption,[39] leading to a higher adsorption capacity.

3.3. Quantification of the Adhesion Force. The adhesion forces on the mesoporous TiO_2 and C−TiO_2 were measured by the immobilization of lysozyme clusters on the AFM-tips. The statistical distributions are shown in Figure S5. The adhesion force (F_A in nN), which represents the total force between the protein clusters and the TiO_2 surface, corresponds to the maximum force jump during retraction according to the force−distance curves, as shown in Figure 4c,d as the insets for the typical examples of T700 and C−T700, respectively. In detail, the detected F_A of lysozyme with T300, T500, T600, and T700 are 1.67, 2.78, 4.68, and 10.10 nN, respectively; and those with C−T300, C−T500, C−T600, and C−T700 are 3.57, 6.51, 10.40, and 22.51 nN, respectively. The value of the adhesion force measured by AFM is related to the contact area between the AFM-tip and the surface, and the contact areas can be calculated with the Hertz and Johnson−Kendall−Roberts theories.[40] The calculated contact areas (S_c in m^2) of the lysozyme interacting with T300, T500, T600, and T700 are 0.82×10^{-16}, 1.15×10^{-16}, 1.63×10^{-16}, and 2.72×10^{-16} m^2, respectively. However, the values of S_c are 1.36×10^{-16}, 2.03×10^{-16}, 2.78×10^{-16}, and 4.65×10^{-16} m^2 for lysozyme with C−T300, C−T500, C−T600, and C−T700, respectively.

The linear relationships between F_A and S_c for the systems of lysozyme interacting with mesoporous-TiO_2 (Figure 4c) and C−TiO_2 (Figure 4d) were established, respectively. F_A/S_c (nN$\cdot m^{-2}$) was obtained for T300, T500, T600, and T700 with the values of 2.04×10^{16}, 2.41×10^{16}, 2.87×10^{16}, and 3.71×10^{16} nN$\cdot m^{-2}$, respectively. For C−T300, C−T500, C−T600, and C−T700, the F_A/S_c (nN$\cdot m^{-2}$) values are 2.62×10^{16}, 3.20×10^{16}, 3.74×10^{16}, and 4.84×10^{16} nN$\cdot m^{-2}$, respectively. It was found that the adhesion force per unit contact area between lysozyme and TiO_2 increased after the carbon modification, which is consistent with the increased adsorption amount per unit area discussed in the foregoing section.

3.4. Quantification of the Molecular Interaction Force. The force of a single protein molecule with TiO_2 (*i.e.*, molecular interaction force) was obtained based on the adhesion force per unit contact area measured with AFM (F_A/S_c in nN$\cdot m^{-2}$) combined with the protein adsorption amount per unit area (Num./S'_T in molecule-number$\cdot m^{-2}$). Therefore, the molecular interaction force was acquired by decomposing the adhesion forces of the protein clusters with the surfaces, instead of directly measuring a single protein molecule with the surfaces, which gives an average force and can, therefore, reflect the effect of the overall solid surface at the nanoscale. The relationships between Num./S'_T and F_A/S_c for mesoporous TiO_2 and C−TiO_2 are shown in Figure 4e,f. The slopes in Figure 4e,f represent the adhesion force of one single lysozyme molecule interacting with mesoporous-TiO_2 and C−TiO_2, corresponding to the values of 0.65 and 0.78 nN, respectively. The results showed that the forces of one single lysozyme molecule with mesoporous TiO_2 and C−TiO_2 were constant, which is independent of the pore structures. This observation is consistent with our previous work,[29] and it also indicates that the pore structures cannot be the intrinsic dominant impactor to determine the immobilization and stability of the proteins, as the strong force indicates strong interaction of lysozyme with the solid surface and thus the high stability. The comparison also shows that the force of lysozyme with C−TiO_2 is larger than that with mesoporous TiO_2. It is reasonable as the carbon modification is one kind of hydrophobic treatment, and the hydrophobic surface achieves high attraction interaction with protein because of the hydrophobic force.[21,39,41,42] It indicates that the surface carbon modification played an important role in the interaction between the protein and the solid surfaces, and the carbon modification can enhance the interaction strength, that is, the immobilization and stability of the protein.

Meanwhile, we aim at developing a new method to construct effective coarse-grained (CG) potentials at the mesoscale between molecules and complex surfaces using data from these quantified-AFM measurements. Then, these detected molecular interaction forces, based on the AFM measurements, will be used to develop CG potentials in our future work.

3.5. Effect of the Carbon Coverage on the Molecular Interaction Forces. Based on the above investigation, the molecular interaction force of lysozyme interacting with TiO_2/C−TiO_2 represented one kind of average force. However, the TiO_2 surface modified with carbon shows a heterogeneous surface exposing both carbon and TiO_2, and it is hard to distinguish the contribution from the part of carbon or TiO_2. In order to investigate that, different amounts of the carbon

https://dx.doi.org/10.1021/acs.langmuir.0c01942
Langmuir 2020, 36, 9323−9332

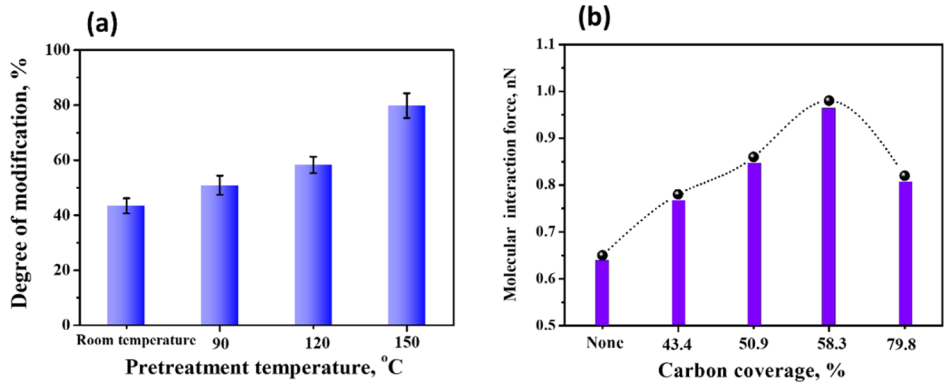

Figure 5. (a) Different carbon coverages obtained by the different pretreatment temperatures; (b) molecular interaction force of a single lysozyme molecule interacting with C−TiO_2 corresponded to the different carbon coverages.

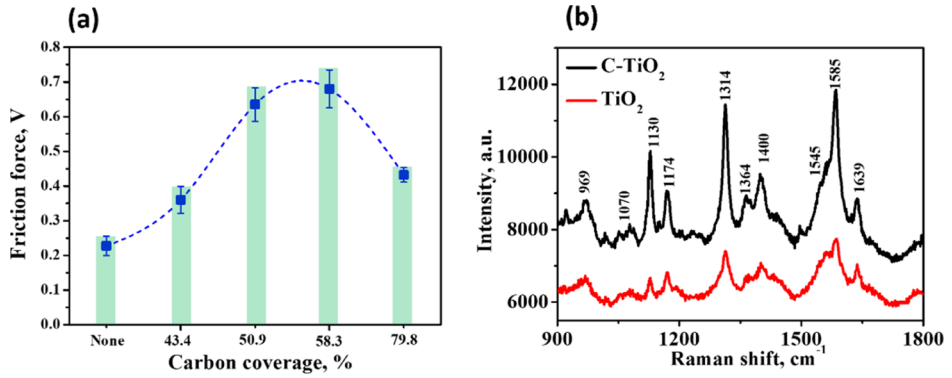

Figure 6. (a) Friction force of lysozyme-coated AFM tip on C−TiO_2 surfaces (T500 as an example) with different carbon coverages; (b) SERS spectra of Cyt C on the TiO_2 and C−TiO_2 substrates.

were modified on the TiO_2 surface to study the effect of the carbon on the molecular interaction force.

Different amounts of carbon modified on the TiO_2 surfaces were obtained by changing the stirring temperature when grafting PPA onto the TiO_2 surface with T500 as an example. The amount of the PPA grafting on the TiO_2 surface increased with the increase of the stirring temperature (see Table S1), leading to the increase of the carbon coverage on the TiO_2 surface after the calcination treatments. After the modification, the pore structures of this C−T500 with different carbon coverages were almost the same according to the overlap pore size distributions (see Figure S6). The SEM and mapping results further indicated the unchanged pore structures and uniform carbon distribution (see Figure S7). The Raman results indicate that the intensities of the graphene increased with increasing the carbon coverages, implying increased electrotransfer properties of C−TiO_2 too (see Figure S8).

Herein, the different carbon coverages on C−TiO_2 were estimated through the amount of phosphorous and calculated according to the XRF data (see Table S1). As shown in Figure 5a, with the increase of the pretreatment temperature, the amount of the carbon on the TiO_2 surface was increased, leading to high carbon coverage. With the treatment at room temperature and 90, 120, and 150 °C, the TiO_2 surface is occupied by the carbon species with values of 43.4, 50.9, 58.3, and 79.8%, respectively. These further assert that the treatment can be regarded as a carbon heterogeneous surface modification.

Based on the measured adsorption capacity of lysozyme onto these C−TiO_2 with different carbon coverages and the adhesion forces by AFM (see Table S2), F_A/S_c and Num./S'_T were obtained. The relationships between F_A/S_c and Num./S'_T for lysozyme onto the C−TiO_2 with different carbon coverages were established, where the slope represents the corresponding force of a single lysozyme molecule interacting with the heterogeneous C−TiO_2 surface (see Figure S9). The molecular interaction forces of lysozyme with heterogeneous C−TiO_2 are about 0.86, 0.98, and 0.82 nN for the carbon coverages of 50.9, 58.3, and 79.8%, respectively (see Figure 5b). As the molecular interaction force of lysozyme depends on the carbon coverage, this force of lysozyme with the heterogeneous C−TiO_2 was determined by the contributions of interacting with both TiO_2 and carbon.

However, it was found that the molecular interaction force increased and then decreased with the increase of the carbon coverage, as shown in Figure 5b. The molecular interaction force was found to be the largest with the carbon coverage of 58.3% with a value of 0.98 nN. When the carbon coverage further increased to 79.8%, the molecular interaction force decreased to 0.82 nN. It indicates that the molecular interaction force is not proportional to the carbon coverage.

For further analysis, the IEPs of these C−TiO_2 were also measured according to the zeta potentials (see Figure S10), and measured values of 3.48, 3.34, 2.89, and 3.16 corresponded to the carbon coverages with 43.4, 50.9, 58.3, and 79.8%, respectively. Those for TiO_2 and carbon are 4.45 and 3.70, respectively. The values of IEPs decreased and then increased with the increase of the carbon coverage, and C−TiO_2 with the carbon coverage of 58.3% reaches the lowest value, indicating the largest negative charges for C−TiO_2 with 58.3% carbon

https://dx.doi.org/10.1021/acs.langmuir.0c01942
Langmuir 2020, 36, 9323−9332

coverage. According to the Derjaguin−Landau−Verwey−Overbeek theory considering both the electrostatic and van der Waals forces, the increase of charges can result in a stronger electrostatic interaction (*i.e.*, molecular interaction force) between protein and surfaces,[43] leading to the force being the largest for C−TiO_2 with 58.3% carbon coverage. The molecular interaction force can directly reflect the immobilization and stability of protein, and thus, the C−TiO_2 samples with the heterogeneous surface exposing about 58.3% carbon and TiO_2 surfaces can achieve high immobilization and stability of the protein with the surfaces.

3.6. Verification of Molecular Interaction Force by the AFM Friction. The friction experiment of AFM measurements can also represent the interaction strength between the fluid and solid surface.[30,44] In order to verify the effect of carbon coverages on the molecular interaction force, the friction force between lysozyme and C−TiO_2 with different carbon coverages was measured. As shown in Figure 6a, the friction force increased and then decreased with increasing the carbon coverages, which is consistent with the results of the molecular interaction forces. The largest friction force was found for C−TiO_2 with the carbon coverage of 58.3%, corresponding to that with the largest molecular interaction force. Meanwhile, both the molecular and friction forces decreased when the carbon coverage increased from 58.3 to 79.8%. It is because the larger molecular interaction force requires more energy to break the interaction to separate the lysozyme-tip from the C−TiO_2 surface, which can strengthen the friction force. The further increased carbon can reduce the frictional property of C−TiO_2, leading to the decreased friction and molecular interaction forces. It also implies that the further increased coverage of carbon can increase the contact probability of the protein with carbon, which can diminish the immobilization and stability of protein, leading to the decreased molecular interaction force.

3.7. Further Applications. The heterogeneous C−TiO_2 materials keep the advantages of both carbon and TiO_2, and the molecular interaction force becomes stronger compared to TiO_2. This implies that such C−TiO_2 materials will own high immobilization and stability of biomolecules as well as high conductivity and can be promising in different applications. In order to illustrate the potential applications of these C−TiO_2, SERS detection and electrochemical biosensors were investigated. For the protein detection, SERS has shown its great advantages in terms of spectral sensitivity and multiplexing for protein detections, where Cyt C is a widely used electron-transfer protein. In this work, Cyt C was used as a typical model protein for SERS measurement. It was found that all the band intensities of Cyt C on C−TiO_2 are stronger compared with those on TiO_2, indicating the enhancement of the electrotransfer properties for C−TiO_2. The reason can be that the modification forms the graphene types of carbon, and the existence of graphene enhances the SERS performance.[45] For biosensors, GOx is an important model system because it is critical for the detection of diabetes. The GOx immobilized on C−TiO_2 and TiO_2 and then the GOx/TiO_2 and GOx/C−TiO_2 were chosen as the sensor electrodes, respectively. It was found that the response current for GOx/C−TiO_2 was found larger than that for GOx/TiO_2, indicating a better electrotransfer property of GOx with C−TiO_2 (see Figure S11). The above investigations implied that these C−TiO_2 materials are promising in practical applications such as in protein detection and biosensing, and further work will be done in the future.

4. CONCLUSIONS

In this work, the effect of partial coverage of carbon on the mesoporous TiO_2 surface on the molecular interaction forces was studied quantitatively and systematically based on the AFM measurements. The heterogeneous carbon modification can remove hydroxyl groups from the TiO_2 surface, without any changes on the geometric and crystalline structures of the TiO_2. The total adsorption capacity and adhesion force of lysozyme molecule with C−TiO_2 are higher than that for the original (unmodified) TiO_2, and the force of a single lysozyme with heterogeneous C−TiO_2 is also stronger than that of unmodified TiO_2. The stronger interaction resulted from two parts: one is the electrostatic force due to the decreased IEPs of C−TiO_2 after modification; the other is the hydrophobic interaction of C−TiO_2 with protein due to the carbon modification. The molecular interaction force is independent of the pore structures but does depend on the varied carbon coverages on the C−TiO_2 surface; it increased and then decreased with the increase of the carbon coverage on the TiO_2 surface, and the carbon coverage with 58.3% achieves the largest molecular and friction forces, where the immobilization and stability of protein is expected to be the best. The carbon coverage with 58.3% was found to be the best coverage degree for the TiO_2−protein system studied in this work. Further investigations of C−TiO_2 in the SERS measurements and electrochemical biosensors indicate that these C−TiO_2 samples with partial coverage can simultaneously keep the advantages of both the hydrophobic carbon and hydrophilic TiO_2 and can, therefore, be a good candidate in the applications of protein detection and biosensing.

■ ASSOCIATED CONTENT

Supporting Information

The Supporting Information is available free of charge at https://pubs.acs.org/doi/10.1021/acs.langmuir.0c01942.

FT-IR and XPS pattern of PPA, mesoporous TiO_2, PPA−TiO_2, and C−TiO_2; zeta potentials of mesoporous TiO_2 and C−TiO_2; photograph of mesoporous TiO_2 and C−TiO_2; SEM and TEM results of C−TiO_2, PPA−TiO_2, and mesoporous TiO_2; distributions of adhesion forces; pore size distributions of C−TiO_2 modified with different carbon coverages; SEM and mapping results of C−TiO_2 modified with different carbon coverages; Raman spectrum of C−TiO_2 modified with different carbon coverages; P_2O_5 XRF results of the content of PPA−TiO_2 and C−TiO_2; adsorption capacity and adhesion force of protein onto C−TiO_2 with different carbon coverages; molecular interaction force of the protein with C−TiO_2 with different carbon coverages; zeta potentials of C−TiO_2 with different carbon coverages; and electrochemical biosensor data of the protein with TiO_2 and C−TiO_2 (PDF)

■ AUTHOR INFORMATION

Corresponding Authors

Xiaoyan Ji − *Energy Engineering, Division of Energy Science, Luleå University of Technology, 97187 Luleå, Sweden*; Email: xiaoyan.ji@ltu.se

Xiaohua Lu − *State Key Laboratory of Materials-Oriented Chemical Engineering, Nanjing Tech University, Nanjing 210009, P.R. China*; orcid.org/0000-0001-9244-6808; Email: xhlu@njtech.edu.cn

https://dx.doi.org/10.1021/acs.langmuir.0c01942
Langmuir 2020, 36, 9323−9332

Authors

Yihui Dong − *State Key Laboratory of Materials-Oriented Chemical Engineering, Nanjing Tech University, Nanjing 210009, P.R. China*

Aatto Laaksonen − *State Key Laboratory of Materials-Oriented Chemical Engineering, Nanjing Tech University, Nanjing 210009, P.R. China; Department of Materials and Environmental Chemistry, Arrhenius Laboratory, Stockholm University, SE-10691 Stockholm, Sweden; Centre of Advanced Research in Bionanoconjugates and Biopolymers, Petru Poni Institute of Macromolecular Chemistry, 700487 Iasi, Romania*

Wei Cao − *School of Chemistry, Tel Aviv University, Tel Aviv 69978, Israel;* orcid.org/0000-0001-5227-7632

Hongyan He − *CAS Key Laboratory of Green Process and Engineering, State Key Laboratory of Multiphase Complex Systems, Beijing Key Laboratory of Ionic Liquids Clean Process, Institute of Process Engineering, Chinese Academy of Sciences, Beijing 100190, P. R. China;* orcid.org/0000-0003-1291-2771

Complete contact information is available at: https://pubs.acs.org/10.1021/acs.langmuir.0c01942

Notes

The authors declare no competing financial interest.

■ ACKNOWLEDGMENTS

This work was supported by the National Natural Science Foundation of China Grants (grant nos. 21838004, 21776278). A.L. thanks the Swedish Science Council (VR) and for partial support by a grant from the Ministry of Research and Innovation of Romania, CNCS—UEFISCDI, project number PN-III-P4-ID-PCCF-2016-0050, within PNCDI III. W.C. acknowledges the fellowship from the Sackler Center for Computational Molecular and Materials Science at Tel Aviv University and from the Foreign Postdoctoral Fellowship Program of the Israel Academy of Sciences and Humanities.

■ REFERENCES

(1) Willner, I. Biomaterials for sensors, fuel cells, and circuitry. *Science* **2002**, *298*, 2407−2408.

(2) Howes, P. D.; Chandrawati, R.; Stevens, M. M. Colloidal nanoparticles as advanced biological sensors. *Science* **2014**, *346*, 1247390.

(3) Rajh, T.; Dimitrijevic, N. M.; Bissonnette, M.; Koritarov, T.; Konda, V. Titanium dioxide in the service of the biomedical revolution. *Chem. Rev.* **2014**, *114*, 10177−10216.

(4) Nichols, S. P.; Koh, A.; Storm, W. L.; Shin, J. H.; Schoenfisch, M. H. Biocompatible Materials for Continuous Glucose Monitoring Devices. *Chem. Rev.* **2013**, *113*, 2528−2549.

(5) Shahgaldi, S.; Hamelin, J. Stability study of ultra-low Pt thin film on TiO_2-C core-shell structure and TiO2 encapsulated in carbon nanospheres as cathode catalyst in PEMFC. *Fuel* **2015**, *150*, 645−655.

(6) Zhuang, W.; Zhang, Y.; Zhu, J.; An, R.; Li, B.; Mu, L.; Ying, H.; Wu, J.; Zhou, J.; Chen, Y.; Lu, X. Influences of geometrical topography and surface chemistry on the stable immobilization of adenosine deaminase on mesoporous TiO_2. *Chem. Eng. Sci.* **2016**, *139*, 142−151.

(7) Zhou, Z.; Hartmann, M. Progress in enzyme immobilization in ordered mesoporous materials and related applications. *Chem. Soc. Rev.* **2013**, *42*, 3894−3912.

(8) Sigal, G. B.; Mrksich, M.; Whitesides, G. M. Effect of surface wettability on the adsorption of proteins and detergents. *J. Am. Chem. Soc.* **1998**, *120*, 3464−3473.

(9) Sassolas, A.; Blum, L. J.; Leca-Bouvier, B. D. Immobilization strategies to develop enzymatic biosensors. *Biotechnol. Adv.* **2012**, *30*, 489−511.

(10) Wu, J. C. Y.; Hutchings, C. H.; Lindsay, M. J.; Werner, C. J.; Bundy, B. C. Enhanced Enzyme Stability Through Site-Directed Covalent Immobilization. *J. Biotechnol.* **2015**, *193*, 83−90.

(11) Barbosa, O.; Ortiz, C.; Berenguer-Murcia, Á.; Torres, R.; Rodrigues, R. C.; Fernandez-Lafuente, R. Glutaraldehyde in bio-catalysts design: a useful crosslinker and a versatile tool in enzyme immobilization. *RSC Adv.* **2014**, *4*, 1583−1600.

(12) Brodbeck, W. G.; Nakayama, Y.; Matsuda, T.; Colton, E.; Ziats, N. P.; Anderson, J. M. Biomaterial surface chemistry dictates adherent monocyte/macrophage cytokine expression in vitro. *Cytokine* **2002**, *18*, 311−319.

(13) Roach, P.; Farrar, D.; Perry, C. C. Interpretation of protein adsorption: Surface-induced conformational changes. *J. Am. Chem. Soc.* **2005**, *127*, 8168−8173.

(14) An, R.; Zhuang, W.; Yang, Z.; Lu, X.; Zhu, J.; Wang, Y.; Dong, Y.; Wu, N. Protein adsorptive behavior on mesoporous titanium dioxide determined by geometrical topography. *Chem. Eng. Sci.* **2014**, *117*, 146−155.

(15) Liu, C.; Guo, Y.; Hong, Q.; Rao, C.; Zhang, H.; Dong, Y.; Huang, L.; Lu, X.; Bao, N. Bovine Serum Albumin Adsorption in Mesoporous Titanium Dioxide: Pore Size and Pore Chemistry Effect. *Langmuir* **2016**, *32*, 3995−4003.

(16) Chen, D.; Tang, L.; Li, J. Graphene-based materials in electrochemistry. *Chem. Soc. Rev.* **2010**, *39*, 3157−3180.

(17) Wang, Z.; Dai, Z. Carbon nanomaterial-based electrochemical biosensors: an overview. *Nanoscale* **2015**, *7*, 6420−6431.

(18) Shannnigarn, S.; Gedanken, A. Carbon-coated anatase TiO_2 nanocomposite as a high-performance electrocatalyst support. *Small* **2007**, *3*, 1189−1193.

(19) Yan, X.; Li, Y.; Du, F.; Zhu, K.; Zhang, Y.; Su, A.; Chen, G.; Wei, Y. Synthesis and optimizable electrochemical performance of reduced graphene oxide wrapped mesoporous TiO_2 microspheres. *Nanoscale* **2014**, *6*, 4108−4116.

(20) Topoglidis, E.; Kolozoff, P.-A.; Tiflidis, C.; Papavasiliou, J.; Sakellis, E. Adsorption and electrochemical behavior of Cyt-c on carbon nanotubes/TiO2 nanocomposite films fabricated at various annealing temperatures. *Colloid Polym. Sci.* **2018**, *296*, 1353−1364.

(21) Poland, C. A.; Duffin, R.; Kinloch, I.; Maynard, A.; Wallace, W. A. H.; Seaton, A.; Stone, V.; Brown, S.; MacNee, W.; Donaldson, K. Carbon nanotubes introduced into the abdominal cavity of mice show asbestos-like pathogenicity in a pilot study. *Nat. Nanotechnol.* **2008**, *3*, 423−428.

(22) Jang, H. D.; Kim, S. K.; Chang, H.; Roh, K.-M.; Choi, J.-W.; Huang, J. A glucose biosensor based on TiO2-Graphene composite. *Biosens. Bioelectron.* **2012**, *38*, 184−188.

(23) Xu, J.; Yang, L.; Han, Y.; Wang, Y.; Zhou, X.; Gao, Z.; Song, Y.-Y.; Schmuki, P. Carbon-Decorated TiO2 Nanotube Membranes: A Renewable Nanofilter for Charge-Selective Enrichment of Proteins. *ACS Appl. Mater. Interfaces* **2016**, *8*, 21997−22004.

(24) Im, J.; Kang, J.; Lee, M.; Kim, B.; Hong, S. Selective adsorption and alignment behaviors of double- and multiwalled carbon nanotubes on bare Au and SiO2 surfaces. *J. Phys. Chem. B* **2006**, *110*, 12839−12842.

(25) Jian, G.; Liu, Y.; He, X.; Chen, L.; Zhang, Y. Click chemistry: a new facile and efficient strategy for the preparation of Fe3O4 nanoparticles covalently functionalized with IDA-Cu and their application in the depletion of abundant protein in blood samples. *Nanoscale* **2012**, *4*, 6336−6342.

(26) Bayne, L.; Ulijn, R. V.; Halling, P. J. Effect of pore size on the performance of immobilised enzymes. *Chem. Soc. Rev.* **2013**, *42*, 9000−9010.

(27) Vashist, S. K.; Lam, E.; Hrapovic, S.; Male, K. B.; Luong, J. H. T. Immobilization of Antibodies and Enzymes on 3-Aminopropyl-triethoxysilane-Functionalized Bioanalytical Platforms for Biosensors and Diagnostics. *Chem. Rev.* **2014**, *114*, 11083−11130.

(28) Dong, Y.; Ji, X.; Laaksonen, A.; Cao, W.; An, R.; Lu, L.; Lu, X. Determination of the small amount of proteins interacting with TiO_2 nanotubes by AFM-measurement. *Biomaterials* **2019**, *192*, 368−376.
(29) Dong, Y.; An, R.; Zhao, S.; Cao, W.; Huang, L.; Zhuang, W.; Lu, L.; Lu, X. Molecular Interactions of Protein with TiO2 by the AFM-Measured Adhesion Force. *Langmuir* **2017**, *33*, 11626−11634.
(30) Dong, Y.; Laaksonen, A.; Cao, W.; Ji, X.; Lu, X. AFM Study of pH-Dependent Adhesion of Single Protein to TiO2 Surface. *Adv. Mater. Interfaces* **2019**, *6*, 1900411.
(31) Li, W.; Liu, C.; Zhou, Y.; Bai, Y.; Feng, X.; Yang, Z.; Lu, L.; Lu, X.; Chan, K.-Y. Enhanced Photocatalytic Activity in Anatase/TiO_2(B) Core-Shell Nanofiber. *J. Phys. Chem. C* **2008**, *112*, 20539−20545.
(32) He, M.; Lu, X.-H.; Feng, X.; Yu, L.; Yang, Z.-H. A simple approach to mesoporous fibrous titania from potassium dititanate. *Chem. Commun.* **2004**, 2202−2203.
(33) Mutin, P. H.; Guerrero, G.; Vioux, A. Hybrid materials from organophosphorus coupling molecules. *J. Mater. Chem.* **2005**, *15*, 3761−3768.
(34) Wang, M. S.; Palmer, L. B.; Schwartz, J. D.; Razatos, A. Evaluating protein attraction and adhesion to biomaterials with the atomic force microscope. *Langmuir* **2004**, *20*, 7753−7759.
(35) Li, L.; Zhu, Y.; Lu, X.; Wei, M.; Zhuang, W.; Yang, Z.; Feng, X. Carbon heterogeneous surface modification on a mesoporous TiO_2-supported catalyst and its enhanced hydrodesulfurization performance. *Chem. Commun.* **2012**, *48*, 11525−11527.
(36) Ferrari, A. C.; Meyer, J. C.; Scardaci, V.; Casiraghi, C.; Lazzeri, M.; Mauri, F.; Piscanec, S.; Jiang, D.; Novoselov, K. S.; Roth, S.; Geim, A. K. Raman spectrum of graphene and graphene layers. *Phys. Rev. Lett.* **2006**, *97*, 187401.
(37) Liu, W.; Wang, J.-g.; Li, W.; Guo, X.; Lu, L.; Lu, X.; Feng, X.; Liu, C.; Yang, Z. A shortcut for evaluating activities of TiO_2 facets: water dissociative chemisorption on TiO_2-B (100) and (001). *Phys. Chem. Chem. Phys.* **2010**, *12*, 8721−8727.
(38) Huang, L.; Gubbins, K. E.; Li, L.; Lu, X. Water on Titanium Dioxide Surface: A Revisiting by Reactive Molecular Dynamics Simulations. *Langmuir* **2014**, *30*, 14832−14840.
(39) Nel, A. E.; Mädler, L.; Velegol, D.; Xia, T.; Hoek, E. M. V.; Somasundaran, P.; Klaessig, F.; Castranova, V.; Thompson, M. Understanding biophysicochemical interactions at the nano-bio interface. *Nat. Mater.* **2009**, *8*, 543−557.
(40) Johnson, K. L.; Johnson, K. L. *Contact Mechanics*; Cambridge University Press, 1987.
(41) Wong-Ekkabut, J.; Baoukina, S.; Triampo, W.; Tang, I.-M.; Tieleman, D. P.; Monticelli, L. Computer simulation study of fullerene translocation through lipid membranes. *Nat. Nanotechnol.* **2008**, *3*, 363−368.
(42) Verma, A.; Uzun, O.; Hu, Y.; Hu, Y.; Han, H.-S.; Watson, N.; Chen, S.; Irvine, D. J.; Stellacci, F. Surface-structure-regulated cell-membrane penetration by monolayer-protected nanoparticles. *Nat. Mater.* **2008**, *7*, 588−595.
(43) Butt, H.-J.; Cappella, B.; Kappl, M. Force measurements with the atomic force microscope: Technique, interpretation and applications. *Surf. Sci. Rep.* **2005**, *59*, 1−152.
(44) An, R.; Yu, Q.; Zhang, L.; Zhu, Y.; Guo, X.; Fu, S.; Li, L.; Wang, C.; Wu, X.; Liu, C.; Lu, X. Simple physical approach to reducing frictional and adhesive forces on a TiO_2 surface via creating heterogeneous nanopores. *Langmuir* **2012**, *28*, 15270−15277.
(45) Xu, W.; Mao, N.; Zhang, J. Graphene: A Platform for Surface-Enhanced Raman Spectroscopy. *Small* **2013**, *9*, 1206−1224.

https://dx.doi.org/10.1021/acs.langmuir.0c01942
Langmuir 2020, 36, 9323−9332